Interconnected Two-dimensional Arrays of Niobium Nitride Nanocrystals as Stable Lithium Host

Xu Xiao[+],[a] Wei Yao[+],[a, b] Jun Tang[+],[a] Chuanfang Liu,[c] Ruqian Lian,[c] Patrick Urbankowski,[a] Mark Anayee,[a] Shijie He,[a] Jianmin Li,[a] Hao Wang,[a] Yu Gao,[c] Yingjin Wei,[c] and Yury Gogotsi*[a]

The cycle life of rechargeable lithium (Li)-metal batteries is mainly restrained by dendrites growth on the Li-metal anode and fast depletion of the electrolyte. Here, we report on a stable Li-metal anode enabled by interconnected two-dimensional (2D) arrays of niobium nitride (NbN) nanocrystals as the Li host, which exhibits a high Coulombic efficiency (>99%) after 500 cycles. Combining theoretical and experimental analysis, it is inferred that this performance is due to the intrinsic properties of interconnected 2D arrays of NbN nanocrystals, such as thermodynamic stability against Li-metal, high Li affinity, fast Li^+ migration, and Li^+ transport through the porous 2D nanosheets. Coupled with a lithium nickel–manganese–cobalt oxide cathode, full Li-metal batteries were built, which showed high cycling stability under practical conditions – high areal cathode loading $\geq$4 mAh cm^{-2}, low negative/positive (*N/P*) capacity ratio of 3, and lean electrolyte weight to cathode capacity ratio of 3 g Ah^{-1}. Our results indicate that transition metal nitrides with a rationally designed structure may alleviate the challenges of developing dendrite-free Li-metal anodes.

Pursuit of batteries with higher energy density than commercial lithium (Li)-ion batteries lead to increasing interest in Li-metal batteries.[1–3] Lithium metal is one of the most promising anodes, owing to its ultrahigh theoretical capacity of 3860 mAh g^{-1} and low redox potential of −3.04 V versus a standard hydrogen electrode. However, Li dendrite growth, followed by fast depletion of electrolyte during repeated Li plating/stripping, decreases cycle life and creates severe safety hazards, hindering the commercialization of Li-metal batteries.[4–6] Extensive efforts have been made to alleviate this problem, including designing Li hosts,[7–9] controlling the dendrite growth direction,[10] using additives,[11] modifying electrolytes,[12,13] as well as creating artificial solid electrolyte interphase (SEI)[14] and protective layers.[15–17] Notably, the reported full cells with hundreds of cycles are mainly tested under conditions with low areal cathode loading values (< 2 mAh cm^{-2}) and a flooded electrolyte (>60 μL per cell)[1]. In this context, the output energy density is estimated to be less than 60 Wh kg^{-1}, which is far below the target value of 350 Wh kg^{-1} [1]. To maximize the energy density for practical use, full cells should meet the following requirements: areal cathode loading values $\geq$4 mAh cm^{-2}, electrolyte weight to cathode capacity ratios (*E/C*) $\leq$3 g Ah^{-1}, and negative to positive electrode capacity (*N/P*) ratios or cell balances being as low as possible.[18] However, practical full cells satisfying those conditions are rarely reported in research papers.

Recently, two-dimensional (2D) materials have been explored for suppressing Li dendrites growth. For instance, 10 nm-thick 2D MoS_2 film has been demonstrated as a protective layer for a Li-metal anode.[16] A full Li-sulfur battery based on this modified Li-metal anode performed with high energy density even after 1200 cycles. However, it should be noted that in this system Li metal was used in excess and cathode and anode were also inundated with electrolyte. For practical full cells, 2D metallically conducting materials, such as MXenes, with high surface area may be superior candidates as Li hosts, as they allow to precisely control the *N/P* ratio and anode thickness by electrochemical Li deposition. Although a freestanding film $Ti_3C_2T_x$ MXene can have an excellent conductivity of 15,000 S cm^{-1} or higher, a dense film with restacked 2D flakes is not favorable for fast Li migration, especially at high rates.[19] At high current density, Li may accumulate at certain locations and form dendrites because of uneven Li-ion flux during Li plating and stripping.[20–26] Concentration polarization around Li dendrites results in fast consumption of the active Li and electrolyte.[9,17,27] A three-dimensional (3D) assembly of MXenes as a Li host is an option as it demonstrates an improvement in cycling stability.[28] It is reasonable to assume that a flexible substrate consisting of 2D highly conductive and porous materials with high mechanical stability and resistance against Li can provide both, fast electron and ion transport and thus, be an ideal Li host. It should be mentioned that, theoretically, most oxides, sulfides, and halides react with Li and are not good choices for the Li-metal anode.[29] Transition metal nitrides (TMNs), with significantly lower cathodic limits,

[a] Dr. X. Xiao,[+] Prof. Dr. W. Yao,[+] Dr. J. Tang,[+] Dr. P. Urbankowski, M. Anayee, S. He, Dr. J. Li, Dr. H. Wang, Prof. Y. Gogotsi
A. J. Drexel Nanomaterials Institute
Materials Science and Engineering Department
Drexel University, 3141 Chestnut Street
Philadelphia, PA 19104 (USA)
E-mail: gogotsi@drexel.edu
[b] Prof. Dr. W. Yao[+]
School of Materials Science and Engineering
Yancheng Institute of Technology
211 East Jianjun Road, Yancheng, Jiangsu 224051, China
[c] C. Liu, R. Lian, Prof. Y. Gao, Prof. Y. Wei
Key Lab of Physics & Technology for Advanced Batteries (Ministry of Education),
Jilin University, Changchun 130012, Jilin, China
[+] These authors contributed equally to this work.

Supporting information for this article is available on the WWW under https://doi.org/10.1002/batt.202000186

are thermodynamically stable against Li metal and are predicted to be promising for Li-metal anodes. In addition, TMNs have been demonstrated to be mechanically strong.[30] Nevertheless, the use of TMNs as Li hosts has not been widely explored..[31] This is partially due to the lack of feasible methods for the synthesis of 2D TMNs, leading to challenges in using this promising material system in Li-metal anodes.

In this work, we report on a stable Li-metal anode composed of 2D arrays of NbN nanocrystals as a Li host. Combining advantages of both, zero-dimensional (0D) and 2D morphologies, interconnected 2D arrays of few-nanometer NbN nanocrystals were synthesized using a topochemical method in ammonia on a salt template,[32] providing both high metallic conductivity and abundant ion transport channels. With 10% Ti_3C_2 MXene as a conductive binder, which also helps improve the mechanical strength of the film,[33] a flexible freestanding NbN-based host was fabricated followed by electrochemical Li deposition to precisely load and tune the Li amount, forming a Li-metal anode. This anode could be cycled with higher than 99% Coulombic efficiency (CE) for at least 500 Li plating/stripping cycles. Paired with a lithium nickel–manganese–cobalt oxide (NMC 811) cathode, practical Li-metal batteries were assembled and tested under realistic conditions, maintaining stable performance.

This work is based on a hypothesis explained in Figure 1a and 1b, which compare the proposed mechanisms of Li deposition in 2D arrays of NbN nanocrystals and on a traditional Cu substrate. On the Cu substrate, large amount of Li^+ ions accumulate around pores of the separator after going through it,[20] as shown in Figure 1a. Such an uneven and anisotropic distribution of Li^+ leads to a nonuniform deposition of Li, which in turn accelerates the dendrite growth in the following Li plating/stripping cycles. For the film composed of

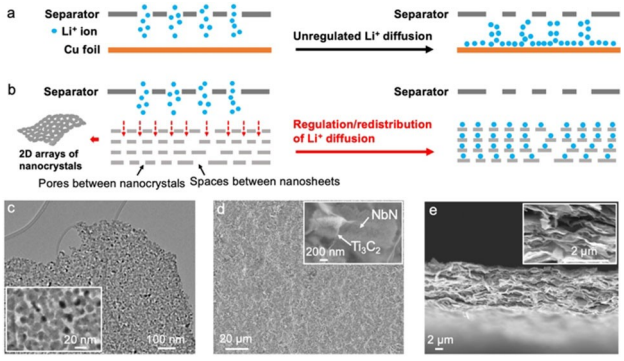

Figure 1. Proposed lithium deposition mechanism and characterization of 2D arrays of NbN nanocrystals used as a Li host. a) The schematic shows the Li deposition process on Cu substrate. Li^+ ions accumulate around the pores of the separator causing nonuniform growth of Li metal. b) The schematic shows an electrode made of stacked porous 2D arrays of nanocrystals. During Li deposition, Li^+ ions can quickly diffuse and penetrate the host through the spaces between nanosheets and pores between nanocrystals, resulting in uniform Li deposition. c) TEM image of a 2D array of NbN nanocrystals. The inset is a higher-resolution TEM image. d) Top-view SEM image of a NbN-based host before lithiation. The inset shows NbN and Ti_3C_2 flakes. e) Cross-sectional SEM image of a freestanding NbN-based host before lithiation. The inset shows the open porous structure of the NbN-based host.

NbN, first, when Li^+ migrates onto the surface of the film, the good affinity of Li to NbN ensures the rapid horizontal diffusion of Li^+ on the surface of each NbN nanocrystals. Then, since the spaces between nanosheets and pores between interconnected nanocrystals are both available for Li^+ transport, large amount of Li^+ can quickly penetrate through film in the vertical direction. Due to the fast and even Li-ion flux from the regulation/redistribution of Li^+ diffusion, the distribution of Li^+ ions in the NbN-based host is uniform as shown in Figure 1b. As a result, an even, continuous, and mechanically strong SEI is expected to form on NbN. A combination of thermal and mechanical stability, as well as high conductivity of NbN that can lower the nucleation energy, leading to stable performance of the anode over many Li plating/stripping cycles.

The synthesis of 2D arrays of NbN nanocrystals was achieved by salt-templating method.[32,34] During topochemical synthesis in a constant flow of ammonia, a thin layer of precursor on the surface of the salt-template was first transformed into 2D transition metal oxide nanosheet and then etched (because of the substitution of O by N) and recrystallized at elevated temperature to form 2D arrays of interconnected NbN nanocrystals with few-nanometer size.[32] According to the transmission electron microscope (TEM) image (Figure 1c), the overall morphology is that of a 2D nanosheet, which consists of interconnected nanocrystals with an average size of 10 nm (inset of Figure 1c and Figure S1). Since flexible 2D films are highly favorable as they can endure the strain caused by Li deposition and expansion,[8,14] vacuum-assisted filtration was used to fabricate a flexible NbN-based film. To enhance the mechanical stability and electrical conductivity, 10 wt. % Ti_3C_2 (Figure S2) was added as a binder,[33] because a pure NbN film was brittle. 2D arrays of NbN and Ti_3C_2 mixed well in the as-fabricated film as confirmed by scanning electron microscopy (SEM) image (Figure 1d). The film was very flexible with no obvious cracking after bending (Figure S3). According to a cross-sectional SEM image (Figure 1e), freestanding NbN films had an open structure, which is advantageous for fast electrolyte penetration and ion diffusion (inset of Figure 1e).

The electrochemical performance of 2D arrays of NbN nanocrystals as the Li host was systematically studied (see detailed information in Table S1). We first deposited 1 mAh cm^{-2} Li into a NbN-based host at 1 mA cm^{-2} (NbN-based host as cathode, Li foil as the anode, denoted as Li||NbN cell) after precycling for tens of Li plating/stripping cycles (see detailed information in Table S1). As shown in the top-view SEM images (Figure 2a), the surface of the electrode was smooth, with no Li dendrites. Lithium uniformly covered each NbN nanosheet while maintaining the electrode morphology, validating our assumption that such an electrode structure can accommodate Li. The voltage profiles of Li plating/stripping of the NbN-based host (current: 1 mA cm^{-2}, Li plating/stripping for 1 h each) are shown in Figure 2b. Coulombic efficiency was $\geq$99%. In general, there are three important potentials for voltage profiles of Li plating/stripping: tip potential (μ_{tip}), nucleation overpotential (μ_{nuc}) and mass-transfer controlled potential (μ_{mtc})[14]. Here, a NbN-based electrode showed a very low μ_{mtc} of 11 mV and μ_{nuc} of 25 mV (inset of Figure 2b).

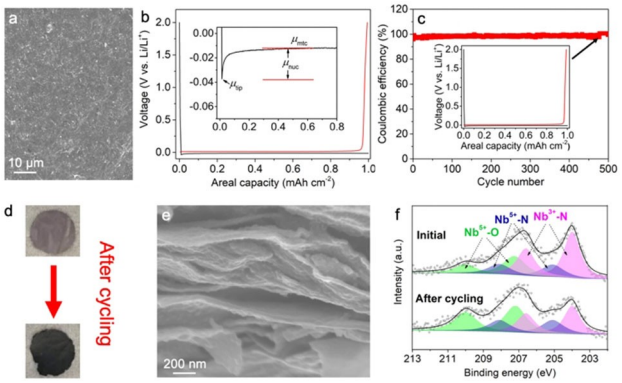

Figure 2. Characterization and electrochemical performance of NbN-based electrodes. a) Top-view SEM image of a NbN-based host after Li deposition of 1 mAh cm^{-2}. No Li dendrites are observed. b) Voltage profiles of Li plating/stripping of NbN-based host at 1 mA cm^{-2} for 1 mAh cm^{-2}. The inset shows three potentials: tip potential (μ_{tip}), mass-transfer controlled potential (μ_{mtc}), and nucleation potential (μ_{nuc}). c) Long-term Li plating/stripping tests of Coulombic efficiency of NbN-based host at 1 mA cm^{-2} for 1 mAh cm^{-2}. The inset shows the voltage profiles of Li plating/stripping of the NbN-based host at the 500th cycle. d) The optical image of the circular NbN electrode before (top) and after (bottom) cycling. e) Cross-sectional SEM image of a NbN-based host (delithiated) after Li plating/stripping for 500 cycles. 2D morphology of the flakes was maintained with a SEI layer formation. f) XPS spectra (Nb 3d orbit) of a NbN electrode before (top) and after (bottom) Li plating/stripping for 500 cycles.

Quantitatively, μ_{nuc} determines the extent to which Li atoms nucleate on the Li host. Here a low μ_{nuc} implies a high Li affinity to NbN. On the other hand, μ_{mtc} reflects how Li migrates on a host in a steady-state process, with lower values indicating fast migration of Li on the surface of NbN. In addition, when tested in a symmetric cell, the NbN-based host was cycled with a low overpotential (Figure S5).

The Li plating/stripping cycling (Li||NbN cell, current: 1 mA cm^{-2}, Li plating/stripping for 1 h each) results are shown in Figure 2c. The NbN-based host showed a high Coulombic efficiency of 99.1% after 500 cycles (inset of Figure 2c). Furthermore, the stability of the electrode structure and composition was verified by SEM and X-ray photoelectron spectroscopy (XPS) (Figure 2e and 2f) before and after 500 cycles of Li plating/stripping (current: 1 mA cm^{-2}, Li plating/stripping for 1 h each). According to the SEM analysis (Figure 2e and Figure S6), the morphology of nanosheets was not destroyed, but the surface was covered by a uniform SEI layer, which may be the reason for the darker color of the electrode after cycling (Figure 2d). In the Nb region of the XPS spectrum (Figure 2f), there are three pairs of doublets corresponding to Nb–N, Nb–N–O, and Nb–O bonds, respectively. The species and corresponding positions of all the bonding arrangements are almost identical after cycling, except for insignificant changes in the relative intensities. Overall, ion channels for fast Li ion diffusion in 2D arrays of NbN nanocrystals in the host can provide uniform Li deposition and enable formation of stable SEI layers. Based on the above analysis, we confirmed our hypothesis that 2D arrays of NbN nanocrystals are thermodynamically stable and resistant to reactions with Li, while their unique morphology and mechanical stability helps achieve a uniform Li-ion flux and suppress Li dendrite growth, accommodate Li expansion, and stabilize the SEI layer.

Theoretical calculations were carried out to corroborate the experimental analysis and better understand the interactions between Li and NbN. For instance, nucleation overpotential μ_{nuc} should be in agreement with the binding energy between Li and the host and lower mass-transfer controlled potential μ_{mtc} would indicate a low Li migration barrier. Notably, theoretical studies on the binding energy of Li atoms with transition metal nitrides are rarely reported, nor do studies explain the influence of various surface terminations on transition metal nitrides. Since 2D arrays of NbN nanocrystals were thoroughly washed with deionized water and exposed to air, –OH and =O terminations are expected and are validated as the only two surface moieties on NbN by XPS analysis (Figure 2f and Figs. S4 and S7). The distance between two adjacent Nb atoms is too large to form Nb–O–Nb bridging bonds, thus only Nb=O (O is above Nb) and Nb–OH were considered, as shown in Figure 3a. We first considered bare NbN with no terminations. The Li binding energy of bare NbN is only −0.61 eV (vs. Li–Li binding energy), meaning that bare NbN is not favorable for Li deposition (too close to Li–Li binding energy). For fully O-terminated NbN (NbN–O), the absorbed Li would quickly bond with O to form an in-plane Li–O, resulting in a highly negative Li binding energy of −2.58 eV. In a model with fully -OH terminated NbN (NbN–OH), H that bonded to O (O–H) would be attracted by the adjacent O, resulting in the deformation of the bond angle between O–H and O=Nb. In this case, H repels the adsorption of Li to some extent, decreasing the Li binding ability to a value of −1.67 eV. To better simulate realistic conditions, we built a model with half =O and half -OH terminations on the surface of NbN. A Li binding energy of −2.08 eV was achieved which is much better than graphene (~ −0.58 eV)[14], and comparable to fully O-terminated Ti_3C_2 (see detailed discussion in Supplementary Note 1 and Figs. S8–S12).

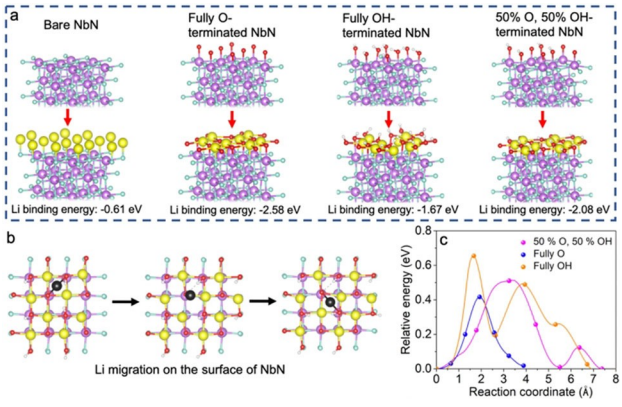

Figure 3. Theoretical calculation of Li binding energy and migration behavior on NbN. The distance between two adjacent Nb atoms is too large to form Nb–O–Nb bridges, and only Nb–O and Nb–OH with O above Nb are considered. a) Binding energy of Li with NbN in different models. b) Simulations of Li migration path in half O, half OH-terminated NbN. Nb, N, O, H, Li and migrated Li are presented by purple, cyan, red, white, yellow, and black spheres, respectively. c) Li migration energy for NbN with different surface terminations.

Although the theoretical model may not exactly match the actual composition of the surface terminations, we obtain trends that may guide further experimental research using the different case scenarios for the surface terminations. Based on the above analysis, it can be concluded that surface chemistry has a great effect on binding energy of Li with NbN, as the presence of O provides active sites for Li absorption while OH decreases the Li binding ability by impeding Li absorption.

In addition, to understand the mechanism behind fast Li migration on the NbN-based host, we further calculated the Li migration energy barrier on NbN surfaces with different terminations (Figure 3b, c, and Figure S13), which was 0.42 eV for NbN–O, 0.68 eV for NbN-OH, and 0.51 eV for NbN with half =O and half -OH terminations. These values are comparable to MoS_2[16] and $Ti_3C_2O_2$.[35] Since a lower migration energy means a lower barrier for Li transport, it is clear that the presence of H hinders Li migration. On the other hand, the unique structure of 2D arrays of NbN nanocrystals, in which the mesopores between nanocrystals facilitate Li transport and work as reservoirs to absorb fresh Li, could further benefit Li migration. As a result, both the low Li migration barrier and unique structure enable the fast Li migration on the NbN-based host.

Considering the high Coulombic efficiency and long-term stability of the Li plating/stripping process within the NbN-based electrode framework, we fabricated a Li-metal full cell using the NbN-based host with deposited Li as an anode, paired with a lithium nickel–manganese-cobalt oxide (NMC 811) cathode. To produce a Li-metal battery with an energy-density higher than 350 Wh kg^{-1} (the target energy density for the next generation of batteries) under practical test conditions, it is recommended that areal capacity of the cathode should be close to or exceed 4 mAh cm^{-2}, with an electrolyte weight to capacity (*E/C*) ratio $\leq$3 g Ah^{-1}, and a low negative to positive electrode capacity (*N/P*) ratio (less than 5 is highly recommended).[15,18] Although several long-term cycling Li-metal batteries have been reported, in general, when constraining the test conditions to the realistic status mentioned above, the cycling performance would quickly degrade to tens of cycles. Accordingly, we first fabricated several full cells under conventional conditions with a Li metal (600 μm thickness) anode, $\geq$3.8 mAh cm^{-2} NMC 811 cathode, and *E/C* ratio of 6 g Ah^{-1} (labeled as bare Li||NMC 811). In this case, the *N/P* ratio is calculated to be more than 20, which is similar to typical values reported in literature. Upon cycling at charge/discharge rates of 0.2 C/0.3 C, only one cell survived 32 cycles, before the capacity suddenly dropped below 80% of the initial capacity (Figure 4a). It should be also noted that the voltage profile of the charge/discharge curve was abnormal, especially regarding fluctuations occurring in the charging curve, resulting in a slow increase of voltage and low Coulombic efficiency (Figure S14). This may be attributed to rapid Li degradation, dendrite growth on a flat Li metal anode, and fast depletion of electrolyte in the bare Li||NMC 811 cell. For comparison, we fabricated full cells using the NbN-based host as a Li host, paired with 4.2 mAh cm^{-2} NMC 811 cathode (see statistical data in Figure S15), with *E/C* ratio of 3 g Ah^{-1} and *N/P* ratio of 3. Here, the thickness of the NbN-based host is ~20 μm, the capacity of the

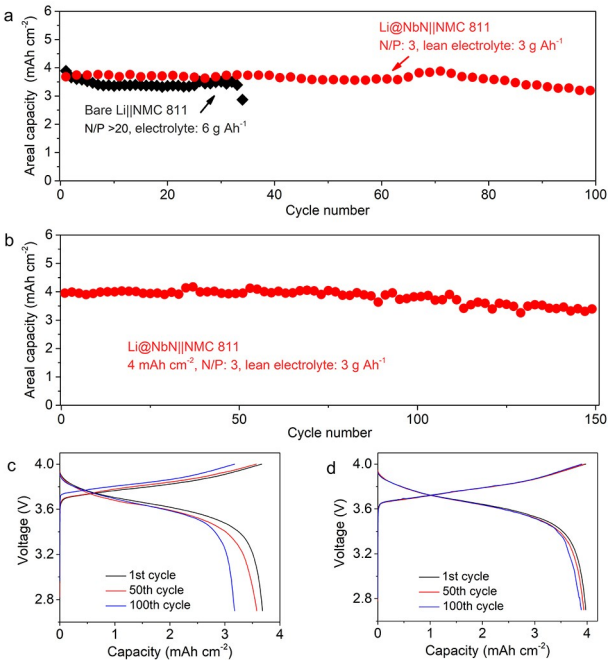

Figure 4. Electrochemical tests of Li@NbN||NMC 811 full cells at practical conditions. Areal capacity: 4 mAh cm^{-2}, negative/positive (*N/P*) capacity ratio: 3, lean electrolyte: 3 g Ah^{-1}. a) Comparison of cycling stability of a Li@NbN||NMC 811 full cell and a bare Li||NMC 811 cell at charge/discharge rates of 0.2 C/0.3 C. The test conditions of bare Li||NMC 811 are conventional, with *N/P* >20 and electrolyte loading of 6 g Ah^{-1}. b) Cycling stability of Li@NbN||NMC 811 full cell at charge/discharge rates of 0.1 C/0.2 C. c–d) Charge-discharge curves of Li@NbN||NMC 811 full cell during the 1st, 50th, and 100th cycles at different rates. c) Charging rate: 0.2 C. Discharging rate: 0.3 C. d) Charging rate: 0.1 C. Discharging rate: 0.2 C. 1 C=6.0 mA cm^{-2}.

NbN-based Li-metal anode was ~2340 mAh g^{-1} with 61 wt% Li in the anode (see detailed information in Table S1). Under the same charge/discharge rate when bare Li||NMC 811 failed after 32 cycles, Li@NbN||NMC 811 achieved 86% retention of initial capacity after 100 cycles (Figure 4a). Unlike bare Li||NMC 811, the voltage profile of the charge/discharge curve of Li@NbN||NMC 811 was maintained during cycling (Figure 4c). Under lower charge/discharge rate, stable cycling was achieved for Li@NbN||NMC 811 cell under such constrained conditions and 85% of initial capacity was retained after 150 cycles (Figure 4b). Note that Li-metal full cells are rarely cycled under such harsh and realistic conditions, as we summarized in Table S2. In addition, the intersection point of the voltage profile of the charge/discharge curves moves just slightly, which is indicative of stable cycling performance (Figure 4d).

Among the three key parameters of Li-metal battery performance (areal capacity of cathode, amount of electrolyte *E/C*, and *N/P* capacity ratio), it is not very difficult to realize a high areal capacity of cathode exceeding 4 mAh cm^{-2} based on commercially available materials, such as lithium nickel–manganese-cobalt oxide, lithium iron phosphate, and sulfur (although the currently reported capacity is mostly 2~3 mAh cm^{-2}, the increasing trend is obvious). However, in general, higher loading of cathode requires a larger amount of Li during each cycle, accelerating the depletion of active Li and formation of SEI on the anode. As a result, rapid consumption

of electrolyte occurs, shortening the battery lifetime. Accordingly, even if a larger amount of electrolyte (6 g Ah^{-1}) is used in the bare Li||NMC 811, it is insufficient to compensate the electrolyte depletion in each cycle, leading to sudden 'death' after tens of cycles. This can also explain why Li-metal full cells that can meet the requirement of low amount of electrolyte and *N/P* ratio simultaneously are rarely reported, as shown in Table S2. An anode host that facilitates fast and uniform Li nucleation, and provides long-term stable cycling is required to match high-capacity cathodes. For the NbN-based host, first, when Li^+ ions diffuse onto host, a fast horizontal (X-direction) Li^+ transport on the surface of NbN nanocrystals occurs due to the strong Li affinity and high Li migration ability (low Li migration barrier). This is followed by the rapid Li^+ diffusion in vertical direction within the host, facilitated by the presence of abundant pores between interconnected nanocrystals and spaces between nanosheets (Figure1b). Such a Li^+ redistribution process, combined with the naturally strong lithiophilicity of metal nitrides[31] and high electron conductivity of NbN-based host (674 S cm^{-1}) that lower the Li nucleation energy,[36] could lead to the fast and uniform Li^+ ion flux, and eventually smooth Li deposition. During the following cycling, fresh Li may migrate into 2D arrays of NbN nanocrystals and compensate for the depletion due to the "self-filling" effect of mesopores.[18] The high electron conductivity of NbN-based electrodes maintains uniform charge distribution, preventing local high current densities that may accelerate the degradation of Li and lead to cracking of SEI.[37] Second, good flexibility, mechanical and thermodynamic stability of NbN-based host help the stabilization of continuous and mechanically strong SEI layers on the interconnected 2D arrays of NbN nanocrystals, which promotes the long-term stable cycling. Accordingly, the NbN-based host meets the requirement for a host for Li-metal due to the intrinsic properties of NbN and unique structure of 2D arrays of interconnected nanocrystals. In addition, the capacity of the NbN-based Li-metal anode was ~2340 mAh g^{-1} (13.5 mAh cm^{-2}), which is much higher than the theoretical capacity of graphite (372 mAh g^{-1}) and practical capacity of commercial silicon-based anodes (less than 1000 mAh g^{-1}). Noting that the thickness of silicon-based and graphite anode is normally 50–120 μm for areal capacity around 3 mAh cm^{-2}. The usage of thin NbN-based host may be advantageous for boosting the volumetric energy density, as recently demonstrated by Ag–C anode with thickness of 5–10 μm.[36] Considering the high electron conductivity of NbN-based host, we assume the removal of current collector may be possible in the future, which could further improve the volumetric energy density of the cell. We have previously reported the use of similar NbN porous arrays in Li–S battery cathodes.[32] Combined with the results reported above, there is a possibility to design a Li–S battery with both electrodes utilizing NbN or other TMN arrays as frameworks for both, Li and S deposition.

In conclusion, we report on a stable Li-metal anode achieved by using interconnected 2D arrays of NbN nanocrystals as a Li host. Combining theoretical and experimental analysis, we demonstrate that a NbN-based host is thermodynamically stable against Li. The high affinity to Li, low Li migration barrier, and mesopores between nanocrystals redistribute and facilitate the Li^+ transport within the electrode. Benefiting from high in-plane electronic conductivity and good mechanical stability, protective SEI is achieved, leading to long-term cycling stability. By pairing with an NMC 811 cathode, we achieved a high areal capacity (4 mAh cm^{-2}) and good cyclability in a Li-metal battery full cell with constrained conditions, using a lean electrolyte (*E/C* 3 g Ah^{-1}) and low *N/P* ratio of 3. A full cell with bare Li-metal as an anode failed after about 32 cycles even under conventional and less constrained conditions. Our results indicate that porous arrays of metal nitride nanocrystals may be potential candidates as ideal Li hosts to achieve dendrite-free Li-metal anodes, with great promise in realizing high energy-density batteries.

Experimental Section

Experimental details including synthesis, characterizations, theoretical calculation and magnetic measurements can be found in the Supporting Information.

Acknowledgements

X. X., W. Y., and J. T. contributed equally to this work. We would like to thank Dr. Linfan Cui (Aalto University) for schematic drawing and Dr. Christopher Shuck (Drexel University) for XRD analysis. P.U. and Y.G. were supported by the U.S. National Science Foundation under grant number DMR-1310245. Y. W. was supported by the National Natural Science Foundation of China (No. 51972140). M.A. was supported by the U.S. National Science Foundation Graduate Research Fellowship under Grant No. DGE-1646737.

Conflict of Interest

The authors declare no conflict of interest.

Keywords: niobium nitride · lithium metal anode · 2D arrays · MXenes · practical condition

[1] J. Liu, Z. Bao, Y. Cui, E. J. Dufek, J. B. Goodenough, P. Khalifah, Q. Li, B. Y. Liaw, P. Liu, A. Manthiram, Y. S. Meng, V. R. Subramanian, M. F. Toney, V. V. Viswanathan, M. S. Whittingham, J. Xiao, W. Xu, J. Yang, X.-Q. Yang, J.-G. Zhang, *Nat. Energy* **2019**, *4*, 180–186.
[2] C. Yang, L. Zhang, B. Liu, S. Xu, T. Hamann, D. McOwen, J. Dai, W. Luo, Y. Gong, E. D. Wachsman, L. Hu, *Proc. Mont. Acad. Sci.* **2018**, *115*, 3770–3775.
[3] W. Xue, Z. Shi, M. Huang, S. Feng, C. Wang, F. Wang, J. Lopez, B. Qiao, G. Xu, W. Zhang, Y. Dong, R. Gao, Y. Shao-Horn, J. A. Johnson, J. Li, *Energy Environ. Sci.* **2020**, *13*, 212–220.
[4] S. S. Zhang, *ACS Appli. Energy Mater.* **2018**, *1*, 910–920.
[5] M. J. Zachman, Z. Tu, S. Choudhury, L. A. Archer, L. F. Kourkoutis, *Nature* **2018**, *560*, 345–349.
[6] J. Xiao, *Science* **2019**, *366*, 426–427.
[7] X. Wang, W. Zeng, L. Hong, W. Xu, H. Yang, F. Wang, H. Duan, M. Tang, H. Jiang, *Nat. Energy* **2018**, *3*, 227–235.

[8] H. Wang, Y. Liu, Y. Li, Y. Cui, *Electrochem. Energy Rev.* **2019**, *2*, 509–517.
[9] G. Huang, J. Han, F. Zhang, Z. Wang, H. Kashani, K. Watanabe, M. Chen, *Adv. Mater.* **2019**, *31*, 1805334.
[10] Y. Liu, Q. Liu, L. Xin, Y. Liu, F. Yang, E. A. Stach, J. Xie, *Nat. Energy* **2017**, *2*, 17083.
[11] X.-B. Cheng, M.-Q. Zhao, C. Chen, A. Pentecost, K. Maleski, T. Mathis, X.-Q. Zhang, Q. Zhang, J. Jiang, Y. Gogotsi, *Nat. Commun.* **2017**, *8*, 336.
[12] M. Cuisinier, P. E. Cabelguen, B. D. Adams, A. Garsuch, M. Balasubramanian, L. F. Nazar, *Energy Environ. Sci.* **2014**, *7*, 2697–2705.
[13] W. Xu, J. Wang, F. Ding, X. Chen, E. Nasybulin, Y. Zhang, J.-G. Zhang, *Energy Environ. Sci.* **2014**, *7*, 513–537.
[14] M. S. Kim, J.-H. Ryu, Deepika, Y. R. Lim, I. W. Nah, K.-R. Lee, L. A. Archer, W. Il Cho, *Nat. Energy* **2018**, *3*, 889–898.
[15] Y. Zhao, G. Li, Y. Gao, D. Wang, Q. Huang, D. Wang, *ACS Energy Lett.* **2019**, *4*, 1271–1278.
[16] E. Cha, M. D. Patel, J. Park, J. Hwang, V. Prasad, K. Cho, W. Choi, *Nat. Nanotechnol.* **2018**, *13*, 337–344.
[17] N. Li, W. Wei, K. Xie, J. Tan, L. Zhang, X. Luo, K. Yuan, Q. Song, H. Li, C. Shen, E. M. Ryan, L. Liu, B. Wei, *Nano Lett.* **2018**, *18*, 2067–2073.
[18] C. Niu, H. Pan, W. Xu, J. Xiao, J. G. Zhang, L. Luo, C. Wang, D. Mei, J. Meng, X. Wang, Z. Liu, L. Mai, J. Liu, *Nat. Nanotechnol.* **2019**, *14*, 594–601.
[19] X. Xiao, H. Wang, P. Urbankowski, Y. Gogotsi, *Chem. Soc. Rev.* **2018**, *47*, 8744–8765.
[20] C.-Z. Zhao, P.-Y. Chen, R. Zhang, X. Chen, B.-Q. Li, X.-Q. Zhang, X.-B. Cheng, Q. Zhang, *Sci. Adv.* **2018**, *4*, eaat3446.
[21] Z. Yu, D. G. Mackanic, W. Michaels, M. Lee, A. Pei, D. Feng, Q. Zhang, Y. Tsao, C. V. Amanchukwu, X. Yan, H. Wang, S. Chen, K. Liu, J. Kang, J. Qin, Y. Cui, Z. Bao, *Joule* **2019**, *3*, 2761–2776.
[22] H. Ye, S. Xin, Y.-X. Yin, J.-Y. Li, Y.-G. Guo, L.-J. Wan, *J. Am. Chem. Soc.* **2017**, *139*, 5916–5922.
[23] R. Weber, M. Genovese, A. J. Louli, S. Hames, C. Martin, I. G. Hill, J. R. Dahn, *Nat. Energy* **2019**, *4*, 683–689.
[24] C. S. Rustomji, Y. Yang, T. K. Kim, J. Mac, Y. J. Kim, E. Caldwell, H. Chung, Y. S. Meng, *Science* **2017**, *356*, eaal4263.
[25] J. Qian, Y. Li, M. Zhang, R. Luo, F. Wang, Y. Ye, Y. Xing, W. Li, W. Qu, L. Wang, L. Li, Y. Li, F. Wu, R. Chen, *Nano Energy* **2019**, *60*, 866–874.
[26] X. Fan, X. Ji, F. Han, J. Yue, J. Chen, L. Chen, T. Deng, J. Jiang, C. Wang, *Sci. Adv.* **2018**, *4*, eaau9245.
[27] S. Choudhury, D. Vu, A. Warren, M. D. Tikekar, Z. Tu, L. A. Archer, *Proc. Mont. Acad. Sci.* **2018**, *115*, 6620–6625.
[28] X. Zhang, R. Lv, A. Wang, W. Guo, X. Liu, J. Luo, *Angew. Chem. Int. Ed.* **2018**, *57*, 15028–15033.
[29] Y. Zhu, X. He, Y. Mo, *Adv. Sci.* **2017**, *4*, 1600517.
[30] Materials science of carbides, nitrides and borides, NATO Science Series; Y. Gogotsi, R. Andrievski, Eds.; Kluwer: Dordrecht, The Netherlands, **1999**.
[31] L. Luo, J. Li, H. Yaghoobnejad Asl, A. Manthiram, *Adv. Mater.* **2019**, *31*, 1904537.
[32] X. Xiao, H. Wang, W. Bao, P. Urbankowski, L. Yang, Y. Yang, K. Maleski, L. Cui, S. J. L. Billinge, G. Wang, Y. Gogotsi, *Adv. Mater.* **2019**, *31*, e1902393.
[33] N. Sun, Q. Zhu, B. Anasori, P. Zhang, H. Liu, Y. Gogotsi, B. Xu, *Adv. Funct. Mater.* **2019**, *29*, 1906282.
[34] X. Xiao, P. Urbankowski, K. Hantanasirisakul, Y. Yang, S. Sasaki, L. Yang, C. Chen, H. Wang, L. Miao, S. H. Tolbert, S. L. Billinge, H. D. Abruna, S. J. May, Y. Gogotsi, *Adv. Funct. Mater.* **2019**, *29*, 1809001.
[35] Y. Xie, Y. Dall'Agnese, M. Naguib, Y. Gogotsi, M. W. Barsoum, H. L. Zhuang, P. R. C. Kent, *ACS Nano* **2014**, *8*, 9606–9615.
[36] Y.-G. Lee, S. Fujiki, C. Jung, N. Suzuki, N. Yashiro, R. Omoda, D.-S. Ko, T. Shiratsuchi, T. Sugimoto, S. Ryu, J. H. Ku, T. Watanabe, Y. Park, Y. Aihara, D. Im, I. T. Han, *Nat. Energy* **2020**, Doi: 10.1038/s41560-020-0575-z.
[37] D. Zhang, S. Wang, B. Li, Y. Gong, S. Yang, *Adv. Mater.* **2019**, *31*, 1901820.

Manuscript received: August 5, 2020
Revised manuscript received: September 6, 2020
Accepted manuscript online: September 11, 2020
Version of record online: October 14, 2020